Journal of Membrane Science 485 (2015) 69–78

Contents lists available at ScienceDirect

Journal of Membrane Science

journal homepage: www.elsevier.com/locate/memsci

Water vapor permeance: The interplay of feed and permeate activity

S. Koester [a], F. Roghmans [a], M. Wessling [a,b,*]

[a] RWTH Aachen University, Chemical Process Engineering, Turmstrasse 46, D-52064 Aachen, Germany
[b] DWI-Leibniz-Institute for Interactive Materials, RWTH Aachen University, Forckenbeckstrasse 50, D-52056 Aachen, Germany

ARTICLE INFO

Article history:
Received 10 October 2014
Received in revised form
4 March 2015
Accepted 9 March 2015
Available online 17 March 2015

Keywords:
Water vapor
Activity
Downstream pressure
Permeance

ABSTRACT

While the permeance of membranes is typically constant for ideal gases, this behavior changes for non-ideal gases and vapors. Due to swelling of the polymer, its simultaneous softening (plasticization) as well as clustering effects of the penetrant molecules, permeability becomes activity dependent. While most experimental investigations focus on studying the influence of feed activity, permeate activity is often neglected. By means of constant-volume variable-pressure measurements we show the importance of both feed and permeate vapor activity for a system of pure water vapor and a variety of membrane materials. We find that a change in activity can enhance or reduce membrane permeability. Either feed or permeate activity was identified to determine the overall mass transfer. Additionally the membrane support revealed a significant impact on overall mass transport properties. This is surprising since concentration polarization effects known from mixed-gas measurements can be excluded. After more than half a decade of water transport studies, well known systems still render transport properties difficult to comprehend. While we succeed to categorize types of transport behavior, fundamental questions on the origin of the transport complexity remain a challenge for future research. Identification of engineering relationships for further module and process development is established however successfully.

1. Introduction

Over the last decades a broad spectrum of applications for water vapor permeable membranes has developed. Due to optimized manufacturing methods, nowadays materials with remarkable high vapor permeabilities and sufficient selectivities are available. Hereby technical applications like the dehydration of natural gas [1], the dehydration of flue gas [2] as well as the drying of compressed air [3] became economic. In addition the market of functional clothing has experienced a tremendous growth [4]. A recently upcoming market is the application of vapor permeable membranes in building ventilation systems [5–7]. In order to enhance the energy efficiency of those systems, plate-and-frame heat exchangers are replaced by the so-called membrane based enthalpy exchangers. Enthalpy exchangers ensure an indirect contact of fresh air and discharged air via a membrane as it is shown in Fig. 1. Heat and moisture is transferred without mixing both streams.

Specific humidity and temperature typically change along the membrane (see Fig. 1). As a result water vapor activity changes on both sides of the membrane as well. Even though basic simulations use activity independent permeances for rough estimations this rigorous assumption is only valid for permanent gases at low to moderate pressures [8]. In fact, solubility and diffusivity of condensable gases is concentration dependent [9]. Consequently the permeability is a function of both the feed and the permeate activity. While variations in feed activity are addressed in many publications, the influence of permeate activity is often neglected [10–14]. Only few publications consider this effect and report significant impacts [15,16,8]. Azher et al. recently published water vapor permeances of Nafion 115 membranes with a non-linear dependence on membrane thickness [17]. They assume that the effects observed can be explained with an inhomogeneity in swelling and a significant impact of downstream activity.

The scope of this work is to quantify the water transport rates of different potential materials as a function of feed and permeate water vapor activity. In particular, we quantify pure water vapor permeation rates without any concentration polarization influences. By the choice of a large variety of materials, we aim to establish a library of transport patterns and classify them in various categories.

2. Measurement of water vapor permeability

Even though various permeability measurement set-ups can be found in the literature [18] only few seem to be appropriate for the investigation of water vapor permeabilities. Reasons can be found in the thermodynamic properties of water vapor and the strong

* Corresponding author at: RWTH Aachen University, Chemical Process #Engineering, Turmstrasse 46, D-52064 Aachen, Germany. Tel.: +49 241 80 95488.
E-mail address: manuscripts.cvt@avt.rwth-aachen.de (M. Wessling).

http://dx.doi.org/10.1016/j.memsci.2015.03.019
0376-7388/

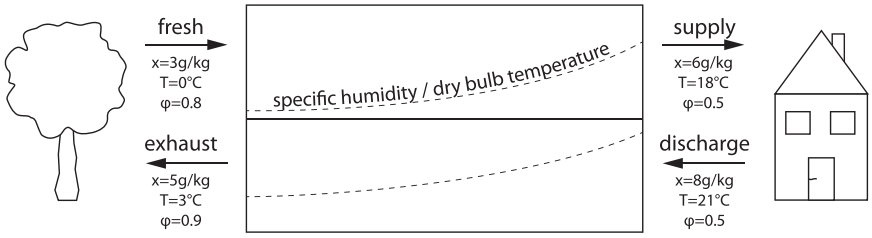

Fig. 1. Humidity profile of enthalpy exchangers in building ventilation systems.

interaction of the vapor molecules [19]. Constant-pressure variable-volume methods are typically operated at a permeate pressure of around 1 atm [20]. Hence the saturation pressure of water vapor limits the application range to temperatures above 100 °C. Main drawbacks of mixed-gas measurements [21] are concomitant fluid dynamics phenomena as well as the need for additional moisture analytics. Applying a gas chromatograph limits the sampling rate. Dew point mirrors make online measurements feasible but the accuracy of those measurements depends strongly on the moisture content. Especially at low vapor transmission the determination of the permeate moisture content is challenging. A widely used and standardized water vapor permeability measurements is the cup method [22,23]. It was solely developed to measure water vapor permeability. Nevertheless this setup is also limited to a certain range of vapor transmission rates. At permeabilities beyond this range either the gravimetric measurement of the absorbed water or the concentration polarization within the boundary layer of the membrane provoke significant errors [24].

Probably the most common technique for a determination of gas permeabilities is the so-called time lag technique. It is a constant-volume variable-pressure measurement performed with a single gas [25]. By drying the membrane and evacuating the permeate chamber before each measurement, a time dependent pressure increase according to Fig. 2 can be observed. This pressure increase can be subdivided into two transient parts and a steady state region in between. While the diffusion coefficient is derived from the first transient part, the slope of the steady state region is proportional to permeability [26]. Even though both parameters are calculated on the basis of the same measurement the expected errors differ significantly. A mathematical estimation reveals that calculating the diffusivity results in a minimum error which is five times larger than the one for permeability measurements [27]. Thus the constant-volume variable-pressure technique has to be handled with care in terms of diffusivity measurements, but is a convincing method for the determination of permeability (Fig. 3).

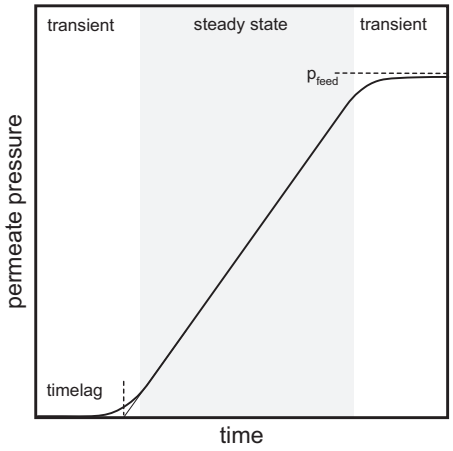

Fig. 2. Permeate pressure as a function of time in an ideal constant-volume variable-pressure measurement.

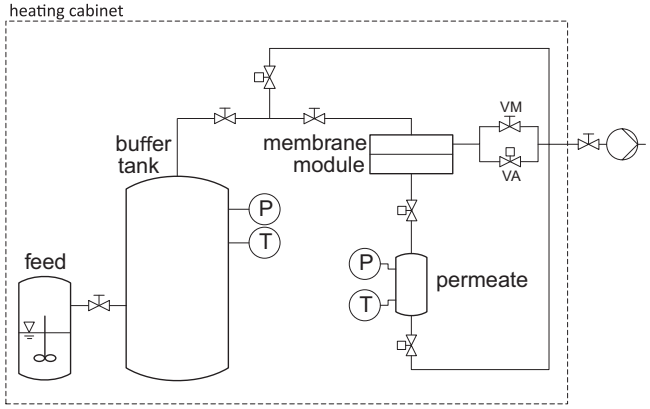

Fig. 3. Experimental setup used for constant-volume variable-pressure measurements.

3. Theory

3.1. Solution diffusion model

The mass transfer through dense membranes is generally given by a linear transport equation

$$J_i = -L_i \cdot \frac{d\mu_i}{dx}. \quad (1)$$

While L_i is a proportionality coefficient, the gradient of chemical potential $d\mu_i/dx$ accounts for the sum of driving forces caused by differences in pressure, temperature and concentration. Due to isothermal conditions any contributions of temperature are neglected.[1]

Hereby the total differential of the chemical potential reduces to

$$d\mu = RTd\ln(a_i) + v_i dp. \quad (2)$$

a_i equals the activity, v_i is the molar volume and p is the pressure. In general the permeation of gases through dense polymeric membranes follows a three step solution diffusion mechanism [29]. After the gas is absorbed on the feed side of the membrane, it diffuses through the polymer and desorbes on the permeate side. The solution-diffusion model assumes that the pressure throughout the whole membrane thickness is constant. Thus $dp=0$ and the transmembrane flux J_i only depends on the activity $a_i = \gamma_i c_i$ of the penetrating molecule. Since the activity coefficient γ_i is unity for low concentrations Eqs. (1) and (2) can be simplified to

$$J_i = -\frac{RTL_i}{c_i}\frac{dc_i}{dx}. \quad (3)$$

[1] Joule–Thomson coefficient at $T=45$ °C is given to $\mu=16.91$ K/bar [28]. With a maximum $\Delta p = 58.4$ mbar (see Table 3) this leads to a theoretical $\Delta T \approx 1$ °C. Since membranes are extremely thin and placed on a sintered filter it is assumed that any ΔT is immediately compensated.

By summarizing RTL_i/c_i to the diffusion coefficient D_i Fick's law of diffusion is being obtained

$$J_i = -D_i \frac{dc_i}{dx}. \tag{4}$$

An integration across the membrane results in

$$J_i = -D_i^* \frac{c_{i,fm} - c_{i,pm}}{\delta} \tag{5}$$

with δ being the membrane thickness. $c_{i,fm}$ and $c_{i,pm}$ indicate the membrane concentration at the feed and permeate interphase respectively. The diffusion coefficient used in Eq. (4) is most often concentration dependent. Thus a mean value D_i^* comprising the diffusion coefficient as a function of membrane thickness is being introduced.

$$D_i^* = \frac{1}{c_{i,fm} - c_{i,pm}} \int_{c_{i,fm}}^{c_{i,pm}} D_i \, dc. \tag{6}$$

Since the concentrations $c_{i,fm}$ and $c_{i,pm}$ within the membrane are not directly accessible, it is common to derive an alternative term for Eq. (5). For this purpose the consistence of the chemical potential at the membrane interphase is being considered. On the feed side it is given by

$$\mu_{i,f} = \mu_{i,fm}. \tag{7}$$

Integration of Eq. (2) for a compressible fluid (gas phase with ideal gas behavior) as well as an incompressible one (membrane phase) leads to

$$\mu_i^0 + RT \ln\frac{p_{i,f}}{p_f} + RT \ln\frac{p_f}{p_{i,sat}} = \mu_i^0 + RT \ln(\gamma_{i,fm} c_{i,fm}) + v_i(p_f - p_{i,sat}). \tag{8}$$

The reference pressure is chosen to be $p_{i,sat}$ in both cases, i.e. the reference chemical potential μ_i^0 is the same on both sides of the equation. Hence the membrane concentration at the feed interphase can be rewritten to

$$c_{i,fm} = \frac{p_{i,f}}{p_{i,sat}\gamma_{i,fm}} \cdot \exp\left(\frac{-v_i(p_f - p_{i,sat})}{RT}\right). \tag{9}$$

As v_i denotes the molar volume of the dissolved gas, the exponential term is assumed to be close to unity for gases with low solubilities. This leads to

$$c_{i,fm} = \frac{p_{i,f}}{\gamma_{i,fm} \cdot p_{i,sat}}. \tag{10}$$

By introducing the sorption coefficient $S_i = 1/(\gamma_{i,fm} \cdot p_{i,sat})$ this equation can further be simplified to

$$c_{i,fm} = S_i \cdot p_{i,f}. \tag{11}$$

The concentration at the permeate interphase is calculated analogical to

$$c_{i,pm} = S_i \cdot p_{i,p}. \tag{12}$$

Summarizing Eq. (5), Eqs. (11) and (12) allow the calculation of the transmembrane flux as a function of partial pressures $p_{i,f}$ and $p_{i,p}$.

$$J = \frac{D_i^* S_i (p_{i,f} - p_{i,p})}{\delta} \tag{13}$$

If the definition of permeability $P_i = D_i^* \cdot S_i$ is considered this term can finally be simplified to

$$J = P_i \cdot \frac{(p_{i,f} - p_{i,p})}{\delta}. \tag{14}$$

It is obvious that the description of mass transfer with permeability (Eq. (14)) is different compared to the one based on solubility and diffusivity (Eq. (14)). Using permeability is less fundamental but much easier to handle. Only with constant diffusion coefficients (Eq. (5)) and linear sorption isotherms (Eqs. (11) and (12)) it is possible to correctly split permeability in single contributions of diffusivity and solubility.

3.2. Constant-volume variable-pressure method

As worked out before a time dependent increase in permeate pressure is the basis for any constant-volume variable-pressure measurement. Since only mass transfer through the membrane accounts for this pressure increase, a mole balance of the permeate chamber is given by

$$J \cdot A_{mem} = \frac{dn_p}{dt}. \tag{15}$$

A_{mem} denotes the active membrane area and n_p equals the number of moles in the permeate. Even though water molecules tend to interact and form hydrogen bonds water vapor behaves like an ideal gas within a certain range of process conditions. The mathematical error is given to 0.1% at a saturation pressure of 10 kPa and 1.6% at a 100 kPa respectively [30]. Considering ideal gas behavior Eq. (15) can be rewritten to

$$J = \frac{dp_p}{dt} \cdot \frac{V}{RT} \cdot \frac{1}{A_{mem}}. \tag{16}$$

Inserting Eq. (14) leads to

$$Pdt = \frac{V}{RT} \cdot \frac{\delta}{A_{mem}} \frac{dp_p}{p_f - p_p(t)}. \tag{17}$$

In general the integration of this term allows the calculation of permeability P. A simple analytical solution is only feasible if the feed pressure and the permeability are constant. This is in direct contrast to the hypothesis of this work. However if very small time intervals ($t \to t^*$) are chosen permeate pressure stays almost constant ($p \to p^*$). As a consequence permeability is assumed to be constant within these intervals as well.

$$P \int_t^{t^*} dt = \frac{V}{RT} \cdot \frac{\delta}{A_{mem}} \int_{p_{p,t}}^{p_{p,t^*}} \frac{dp_p}{p_f - p_p(t)}. \tag{18}$$

Integration of Eq. (18) finally leads to

$$P = \frac{V}{RT} \cdot \frac{\delta}{A_{mem} \cdot (t^* - t)} \cdot \ln\left(\frac{p_f - p_p(t)}{p_f - p_p(t^*)}\right). \tag{19}$$

Hereby calculation of permeability P is possible if information on permeate volume V, temperature T, membrane thickness δ, active membrane area A_{mem}, feed pressure p_f as well as permeate pressure p_p are available. If the membrane thickness is unknown permeance Q can be calculated instead.

$$Q = \frac{P}{\delta} \tag{20}$$

While P is an intrinsic material parameter given in Barrer,[2] the value of the permeance Q is membrane specific. Its unit is GPU[3] (gas permeating units).

4. Experimental

A simplified schematic drawing of the experimental setup is depicted in Fig. 2. It consists of a cylindric test cell containing the membrane sample, a vacuum pump (Vacuubrand RC6) and a total of three stainless steel reservoirs. All components despite the vacuum pump are placed within a heating cabinet (Memmert ULE 600). They are interconnected by a minimum number of pipes, which reduces risk of gas leakages and ensures instantaneous process control.

[2] 1 Barrer = $1e^{-10}$ $cm^2/(s\ cmHg) = 2.7e^{-9}$ $m_N^3/(m\ h\ bar)$.
[3] 1 GPU = 10^{-6} $cm/(s\ cmHg) = 2.7e^{-3} m_N^3/(m^2 h\ bar)$.

Thermocouples (type T) on both sides of the membrane as well as differential pressure sensors (Wika, UT-10) monitor essential process parameters. Accuracy of the measurements is enhanced by choosing pressure sensors with an upper limit of 250 mbar (feed) and 100 mbar (permeate) respectively. Data is logged with a sampling rate of 0.5 s using a SPS (National Instruments FP-1000) in combination with a personal computer. The core of the setup consists of a cylindric test cell. As shown in Fig. 4 the feed flows from the center to the outside. The permeate is being collected and removed in the center of the lower module part. To ensure a sufficient mechanical stability the sample is deposited on top of a sintered metal filter (SIKA R200). In addition a ring-shaped Micro-PES layer (Membrana, 1F-EL) protects the membrane from damages caused by the sintered filter. The o-ring which seals the feed chamber, reduces the diameter of the active membrane layer by approximately 10 mm. This accounts for a 30% decrease of the surface area, which has to be taken into account when analyzing the experimental results.

The accuracy and reproducibility of constant-volume variable-pressure measurements depend significantly on the initial vapor purity. At infinite high purities concentration polarization issues can be neglected. Hereby the experimental procedure is simplified compared to mixed gas measurements [21]. Prior to each measurement the rig is evacuated and flushed thoroughly with water evaporating from the liquid reservoir shown in Fig. 2. At the end of the flushing step, the permeate chamber remains evacuated while the feed pressure is set to the desired vapor activity. Its upper limit is given by the saturation pressure at the heating cabinet temperature. Feed pressures below saturation are obtained by the automatic control valve (VA) located behind the membrane module. Opening this valve reduces the pressure and accelerates the evaporation within the liquid reservoir. As the heat of evaporation is provided by the liquid water itself, the temperature within the liquid reservoir decreases. This leads again to a decline of the evaporation rate. From the description above it is obvious that feed pressure control is a critical issue. In fact, it is hard to account for different activities by means of a single valve. Hence a second manual valve (VM) connected in parallel is used to pre-adjusted the feed pressure. Its setpoint is 5–10 mbar above the desired feed pressure. Consequently the range of the vernier adjustment is minimized resulting in an appropriate automatic control.

As described in Eq. (19) permeance is calculated from the pressure increase in the permeate chamber. Hence the time resolution and hereby the accuracy can be influenced by tuning the size of the permeate chamber. Large volumes imply long measurements. Choosing smaller volumes result in shorter measurements with lower time resolution. All experiments within the course of this work were performed with the two permeate chambers listed in Table 1. Contributions of connectors and valves directly connected to the permeate chamber are already considered. In order to keep the feed pressure constant throughout the entire experiment the size of the feed chamber is recommended to be at least one order of magnitude larger than the permeate chamber. The rig depicted in Fig. 2 comprises two feed chambers with different functions. The liquid reservoir contains water which partly evaporates over time. The contribution of this tank to the overall feed volume is rather small and can be neglected. The second reservoir is a buffer tank with the largest volume (see Table 1). Its main purpose is to dampen any fluctuation in feed pressure caused by permeation and partial evacuation.

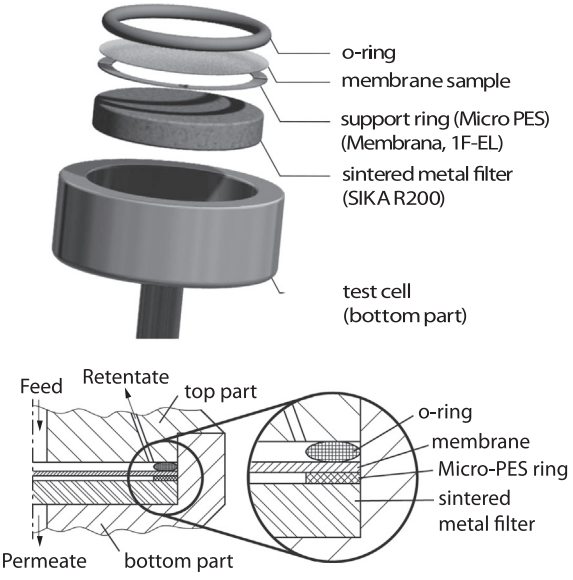

Fig. 4. Three dimensional and cross-sectional schematic of the cylindric permeation cell.

4.1. Materials

An overview of all membranes investigated is given in Table 2. In total, seven materials of five different suppliers were considered. They can be categorized by thickness, structure, the polymer of the separation layer and the type of reinforcement. As concentration polarization effects can be excluded in case of single gas measurements, the polymer of the separation layer and membrane thickness are assumed to be key parameters in terms of permeance. At this point it is important to note that we focus on the interplay of feed and permeate activity. Hence membrane thickness is not used to identify the best performing material with the highest permeability.

The *M2234* sample is delivered by Epurex Films and traded under the brand Platilon®. It is made out of PEBAX and originally applied within functional textiles. PEBAX is a hydrophilic blockcopolymer which consists of rigid polyamide (PA) segments and soft polyethylene oxide (PEO) blocks. The PA segments ensure the mechanical strength while the PEO blocks are predominantly determining transport properties [31].

The *MX4-A* membrane is a polyether polyurethane copolymer on top of a polyethylene substrate [32]. It is distributed by dPoint

Table 1
Specifications of the experimental setup.

Parameter	Range
V_{buffer} (cm^3)	20,000
V_p (cm^3)	230/2133
d_{sample} (mm)	60
d_{mem} (mm)	50

Table 2
Properties of the membrane samples.

Membrane	Supplier[a]	Material	Type[b]	Reinforcement/ support	Thickness[c] (μm)
Dehesive920	DWI	PDMS	h	–	310
M2234	EF	PEBAX	h	–	15
fumasep® FAA-3rf	FT	Polyaromatic	h	e-PTFE	35
fumasep® F-930-rfd	FT	PFSA	h	e-PTFE	30
Mx4-A	DP	Polyether copolymer	c	PE	1–2
POMS	HZG	POMS	c	PAN/PES	5
Polyactive®	HZG	Polyactive	c	PAN/PES	

[a] DP=dPoint, DWI=DWI Leibnitz Institute for Interactive Materials, EF=Epurex Films, FT=FuMA-Tech, HZG=Helmholtz-Zentrum Geesthacht.
[b] c=Composite, h=homogeneous.
[c] Selective layer.

technologies and currently applied within enthalpy exchangers for building ventilation systems.

Polyactive was developed by Helmholtz-Zentrum Geesthacht (HZG) and is commercially distributed by GMT. It combines soft PEO segments with rigid polybutylene terephthalate (PBT) blocks [33]. The ultra-thin selective layer ($\sim$ 50–100 nm) is casted on top of thin PDMS layer ($<$ 300 nm) which is applied on a PAN support [34]. The intermediate PDMS layer is highly permeable and basically smoothens the surface of the porous PAN support. This leads to a reduction in top layer thickness. The PEO-PBT layer is additionally protected by a very thin PDMS top-layer [35].

A second composite materials delivered by HZG is the *POMS* membrane. Its selective layer consists of poly(octyl methylene siloxane) which is again casted on a PAN substrate. POMS is a rubbery polymer typically used in vapor recovery. Compared to PDMS lower permeabilities but higher selectivities have been reported [36].

PDMS films were manufactured on basis of Dehesive920 (Wacker) by DWI – Leibniz Institute for Interactive Materials. Those films are supplied without any reinforcement. Samples are much thicker than all other materials investigated.

The fumasep® *F-930-rfd* is a perfluorosulfonic acid (PFSA) based cation exchange membrane with fixed negative charges and positive mobile counter ions [37]. It is optimized with regard to ion-transport and mainly applied in electrochemical membrane processes. For ion-exchange membranes it is known that the counter-ion influences water vapor transmission [38]. Here the membranes were in H^+ form. Due to its particular manufacturing process the fumasep® F-930-rfd contains some semi-crystalline structures. These transition back to amorphous state cause hysteresis effects which typically lowers experimental reproducibility. Those structural effects are prevented by an additional post-treatment prior to the experiments.

The fumasep® *FAA-3rf* sample is a non-fluorinated aromatic polymer which is also optimized for ion-transport. The anion exchange membrane has fixed positive charges and negative mobile counter ions (Br^-).

4.2. Parameters and data sampling

Fig. 2 depicts an idealized run of the permeate pressure over time in a constant-volume variable-pressure apparatus. However this behavior is only obtained if the initial feed pressure is significantly higher than the permeate pressure. In case of water vapor the maximum feed pressure is limited to saturation pressure. At moderate temperatures around $T=45$ °C its value will not exceed 100 mbar. Hence the feed pressure is close to permeate pressure. Consequently permeate pressure does not increase linearly but deflects over time (Fig. 5).

The question is whether this deflection is only caused by a change in driving force or if permeance also changes as a function of activity. To answer this question constant-volume variable-pressure experiments with different feed and permeate activities were carried out at $T=45°$. This temperature corresponds to a saturation pressure of 95.94 mbar. For each sample feed activity was adjusted to setpoints of $a_f=0.4$, $a_f=0.6$ and $a_f=0.8$ respectively. Permeate pressure was logged continuously over time. As described before the permeance of the material is proportional to the slope of the curve shown in Fig. 5. Thus an activity dependent permeance can be calculated from the data obtained by partially linearizing the graph. For this purpose small intervals are defined in the range of $a_p=0.3\ldots0.9a_f$. The distance between two intervals is $0.1a_f$ and the width of each interval is $\pm0.01a_f$. An overview of all intervals is given in Table 3. In order to obtain statistically profound results a single data point comprises several replications. Each sample is characterized at three different feed activities ($a_f=0.4$, $a_f=0.6$ and $a_f=0.8$). The permeance at a certain feed and permeate activity is calculated from at least four consecutive runs using the same sample. In between two consecutive measurements the permeate reservoir is basically re-evacuated to obtain another pressure increase (see Fig. 6). Finally the data of three different samples is averaged per material.

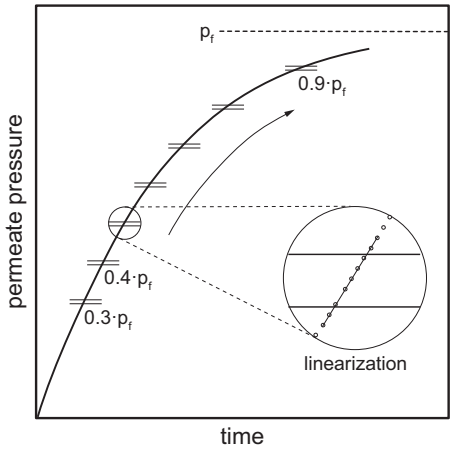

Fig. 5. Permeate pressure as a function of time at low feed pressures.

Table 3
Parameters used for the linear approximations at $T=45°$.

interval	a_f/a_P (–)	p_p (mbar)		
		$a_f=0.4$ $p_f=38.4$ mbar	$a_f=0.6$ $p_f=57.6$ mbar	$a_F=0.8$ $p_f=76.8$ mbar
(0)	0.25	9.2–10.0	13.8–15.0	18.4–20.0[a]
I	0.3	11.1–11.9	16.7–17.8	22.3–23.8
II	0.4	15.0–15.7	22.4–23.6	29.9–31.5
III	0.5	18.8–19.6	28.2–29.4	37.6–39.1
IV	0.6	22.6–23.4	34.0–35.1	45.3–46.8
V	0.7	26.5–27.2	39.7–40.9	53.0–54.5
VI	0.8	30.3–31.1	45.5–46.6	60.6–62.2
VII	0.9	34.2–34.9	51.2–52.4	68.3–69.8

[a] $a_F/a_P=0.25$ only applied for PDMS.

5. Results and discussion

Membranes investigated can be categorized in three groups according to the influence of activity coefficient:

- activity enhanced permeance
- activity reduced permeance
- constant permeance

Below the results of selected materials are presented to visualize the main differences between all groups. The behavior of the remaining materials is briefly summarized.

5.1. Activity enhanced permeance

In the literature permeability data is preferentially reported as a function of pressure difference. The reason is that most researchers focus on a variation of feed pressure while permeate pressure is kept constant. As a consequence permeation data has to be handled with care when used for process design applications [39]. The impact of process conditions can be visualized if permeance of the fumasep® F-930-rfd sample is plotted as a function of pressure difference according to Fig. 7.

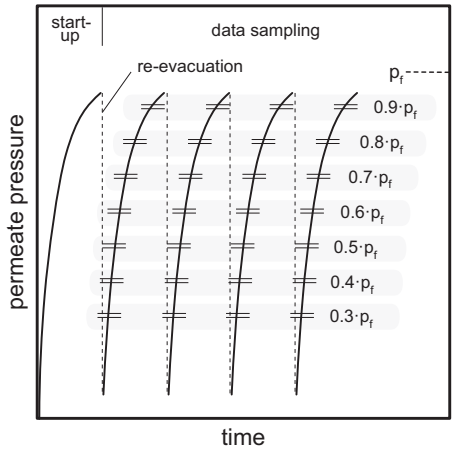

Fig. 6. Data sampling on basis of four consecutive runs; first run is skipped to exclude start-up phenomena.

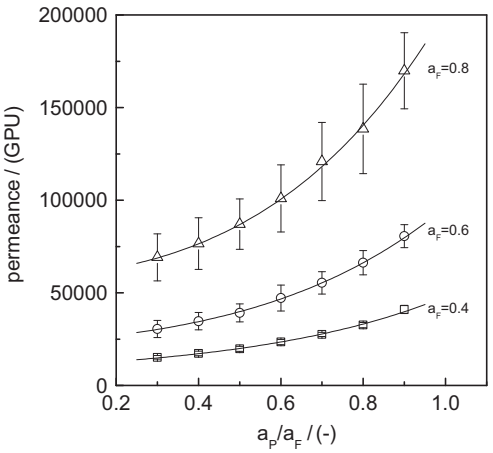

Fig. 8. Water vapor permeance of the fumasep® F-930-rfd sample as a function of feed and permeate activity at T=45 °C sample. (symbols – data points/solid lines – mathematical fitting).

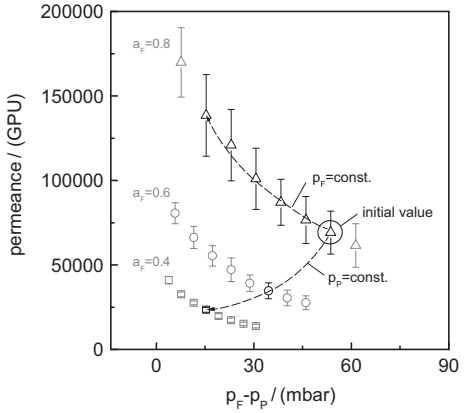

Fig. 7. Water vapor permeance of the fumasep® F-930-rfd sample as a function of partial pressure difference at T=45 °C.

Changing the partial pressure difference from initially 53.7 mbar to 15.3 mbar can either enhance or decrease membrane permeance as shown by the two dashed lines for constant feed or constant permeate pressure. In a first scenario feed activity is kept constant at 0.8 and partial pressure difference is adjusted by increasing permeate activity. This change causes an increase of permeance from 69,000 GPU to 139,000 GPU. In a second scenario permeate activity is kept constant and partial pressure difference is adjusted by a decrease of feed activity. Now, permeance decreases to 23,000 GPU instead. Even though partial pressure difference is the same in both scenarios, permeance varies by more than 600% (23,000 GPU compared to 139,000 GPU). Thus in order to avoid any misinterpretation it is recommended to plot permeance as a function of both feed and permeate activity. The behavior of the fumasep® F-930-rfd is given in Fig. 8. To better visualize the impact of both feed and permeate activities in a single graph a normalized x-axis was introduced. Permeance is plotted over the ratio of permeate to feed activity a_p/a_f. The limits of this x-axis are 0 in the case of an absolute vacuum and 1 if permeate activity equals feed activity. The diagram comprises the results at three different feed activities (a_f=0.4, a_f=0.6 and a_f=0.8). According to Table 3 these activities refer to vapor pressures of p_f=38.4 mbar, p_f=57.6 mbar and p_f=76.8 mbar respectively. Each of the data points represents the average value of three different samples. The error bars indicate the corresponding standard deviation of those three samples.

The fluorinated, PFSA based material shows a significant increase of permeability with feed activity. Referring to Fig. 8 the permeance approximately doubles when the feed activity is increased from a_F=0.4 to a_F=0.6 or from a_F=0.6 to a_F=0.8. Additionally permeance increases with an increase in permeate activity. Changing permeate activity from a_P/a_F=0.3 to a_P/a_F=0.9 leads to a change in permeance by a factor of 2.6. This behavior can be approximated by Eq. (21), which allows a consideration of the actual membrane performance in optimization problems like the one of Scholz [40]. A visualization of the data fitting (Eq. (21)) is given by solid lines in Fig. 8.

$$Q = 3520.7 + 3974.5\frac{a_P}{a_F} + 797.0 \cdot \exp\left[2.36\left(\frac{a_P}{a_F}\right)\right] \times \exp\left[\left(-0.89\left(\frac{a_P}{a_F}\right)^3 + 2.59\left(\frac{a_P}{a_F}\right)^2 - 3.10\frac{a_P}{a_F} + 5.32\right)a_F\right]. \quad (21)$$

The behavior observed is in good agreement with general trends reported in literature. Solubility S as well as diffusivity D were reported to increase for Nafion like materials continuously within activity intervals of 0.2 to 0.9 [41,42]. As permeance depends linearly on the product of both parameters (see Section 3) characteristics like the one depicted in Fig. 8 were expected. A similar behavior was reported by Azher et al. [17]. It is mainly caused by membrane swelling due to exposing the sample to water vapor. Within this study similar trends were observed for the M2234 sample (Epurex films) and the fumasep® FAA-3rf sample (FuMa-Tech). Both samples revealed a dependence of feed as well as permeate activity. The dependence on permeate activity was less pronounced as compared to the fumasep® F-930-rfd sample. Explanations in terms of molecular interpretations go far beyond the scope of this study, however will be essential in future work.

5.2. Activity reduced permeance

Completely different characteristics were observed for PDMS. According to Fig. 9 permeance seems to decrease with both permeate and feed activities. However it is peculiar that the curves of different feed activities a_F diverge at high and low ratios a_P/a_F while they merge in between.

To gain a deeper understanding permeances were additionally plotted as a function of a non-normalized permeate activity (see Fig. 10). From this visualization it is obvious that permeance is predominantly determined by the permeate activity. As a

consequence results can be fitted mathematically without any contribution of the feed activity a_F (Eq. (22)). This is worth to mention since the influence of the feed side is usually assumed to be larger than the one of the permeate side. As shown in Fig. 10 this assumption can lead to errors of 200%.

$$Q = 21.2 + \frac{1453.6}{1+10^{(17.09a_p - 0.15)}} + \frac{69.6}{1+10^{(4.70a_p - 2.76)}} \quad (22)$$

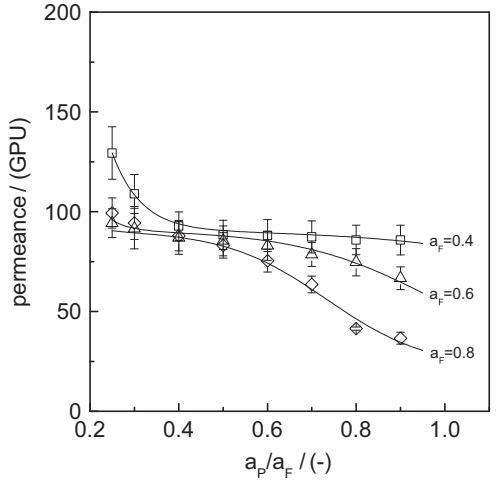

Fig. 9. Water vapor permeance of PDMS at $T=45$ °C as a function of normalized permeate activity a_P/a_F. (symbols – data points/solid lines – mathematical fitting).

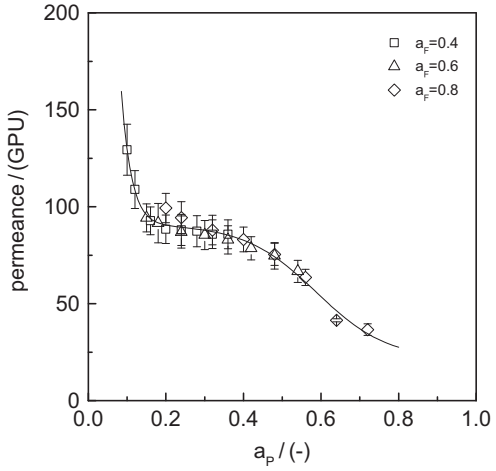

Fig. 10. Water vapor permeance of PDMS at $T=45$ °C as a function of permeate activity a_P. (symbols – data points/solid lines – mathematical fitting).

The sigmoidal shape of the permeance plotted in Fig. 10 indicates that all permeances at different feed activities fall into one master curve. Its remarkable shape requires interpretation. As mentioned before permeability equals the product of solubility and diffusivity. The diffusivity of water vapor in PDMS typically shows an exponential decrease with increasing vapor activities [43,44]. With this knowledge only a sigmoid shaped sorption isotherm causes permeances according to Fig. 10. However the sorption of water vapor in PDMS is typically described with a Flory-Huggins approach [9,45]. A sigmoid shape would only be obtained if dual-mode sorption is superimposed [46]. Thus the combination of diffusion coefficients and sorption data does not offer a conclusive explanation for the results depicted in Fig. 10. Other phenomena like water clustering must have a significant impact on permeance. Clustering is also referred to be the main reason for a reduction of diffusion coefficients with increasing activities [43,44]. The probability of this phenomenon show a strong dependence on vapor activity [43]. Since clustering occurs preferentially at high activities any changes on the downstream side (with initially low activities) might have a dominating impact.

5.3. Constant permeance

As described in Section 4.1 some composite materials were investigated in the course of this study as well. Two different materials belonging to this group are the Polyactive and the POMS sample. The permeances obtained for Polyactive are shown in Fig. 11a. The Polyactive samples do not show any influence of activity. The permeance keeps almost constant at $Q \approx 30.000$GPU. This behavior was not expected since Polyactive itself is a PEO-PBT polymer, which is known to have an activity dependent permeance [47]. Thus other effects beside the polymer of the selective layer are supposed to determine the water vapor transport. In contrast to previous materials (fumasep® F-930-rfd and PDMS) the Polyactive sample is a composite material. It consists of a very thin selective PEO-PBT layer (~ 50–100 nm) which is sandwiched between two PDMS layers, a protection layer and an intermediate layer. The compound of all three layers is supported by a porous PAN layer. If the permeance of the PDMS layers and the PEO-PBT layer are in the same order of magnitude, the PDMS would contribute significantly to the overall transport resistance. From the results plotted in Fig. 9 and

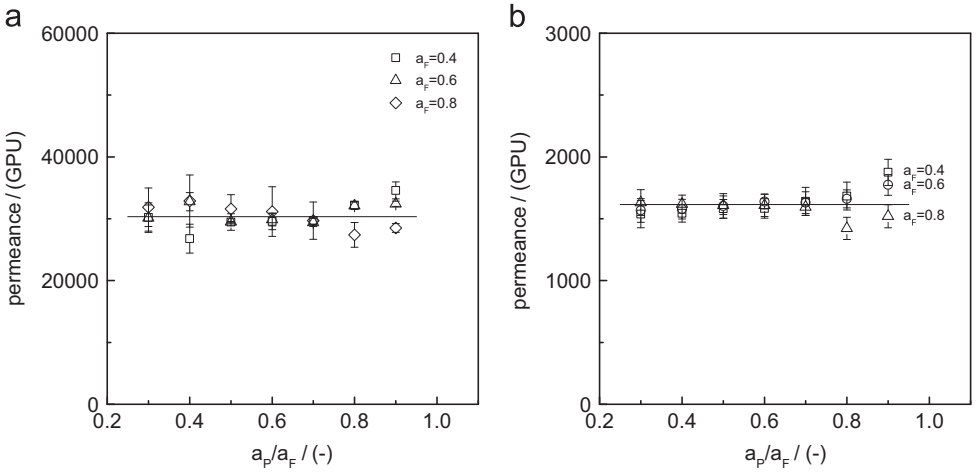

Fig. 11. Water vapor permeance of Polyactive and POMS at $T=45$ °C plotted as the function of a normalized permeate acitivity a_P/a_F. (symbols – data points/solid lines – mathematical fitting). (a) Polyactive, (b) POMS.

the data given in Table 2 the average permeability of PDMS can be calculated to 30,000 barrer. In the literature permeability of PEO-PBT is reported to be around 35,000 barrer [47]. With this data and the knowledge that the PDMS layer is up to six times thicker than the PEO PBT layer, the influence of the PDMS layer on the overall mass transfer resistance can be estimated mathematically. The contribution of the PDMS layer is given by a resistance in series model

$$\frac{R_{PDMS}}{R_{total}} = \frac{R_{PDMS}}{R_{PDMS}+R_{PEO-PBT}} = \frac{6/30,000}{6/30,000+1/35,000} = 0.875. \quad (23)$$

Even with this rough calculation it becomes obvious that the permeance of the PDMS layer is not only contributing to the overall transport resistance but entirely dominant compared to the PEO-PBT top layer.

What remains unresolved is the fact that the permeance of the Polyactive sample is independent of activity. Even if the PEO-PBT behavior is leveling off the PDMS characteristics to a certain extend some activity dependence should be visible. For this reason a second composite material similar to Poylactive was investigated. This material is labeled POMS. The POMS sample consists of a poly(octyl methyl)siloxane layer, which is again on top of a PAN support. Both the PAN support and the POMS layer are significantly thicker compared to the corresponding layers of the Polyactive sample. Additional top layers like PEO-PBT were not applied. The results of the POMS sample are depicted in Fig. 11b. According to sample thickness the permeance of the POMS material is much lower than the one of the Polyactive sample. However it is remarkable that the permeance of the POMS sample is also constant over the entire activity range. Comparing the results of the POMS and Polyactive samples with the behavior of the homogeneous PDMS film leads to the assumption that mass transfer is limited by secondary effects. Possible reasons are the change in film thickness [48,49] or a predominant influence of the support. In order to clarify the impact of the support additional experiments with different membrane configurations were performed.

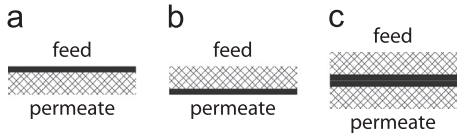

Fig. 12. Membrane configurations. (a) act2feed, (b) act2perm, (c) duplex.

5.4. Influence of the porous support

Constant-volume variable-pressure measurements are independent of concentration polarization effects. This often leads to the hasty conclusion that membrane orientation does not affect the measurement of single gas permeances. However this assumption does not hold if other phenomena like capillary condensation or pressure loss occur within the porous substrate. Zhang recently published simulation results which even reveal that a porous substrate can cause concentration inhomogenities within the selective layer of a composite structure [50]. The question arising is if any of these orientation effects can be visualized by means of single gas measurements. Therefore orientation experiments were carried out using two composite structures namely Polyactive and Mx4-A. In total three different membrane configurations according to Fig. 12 were investigated.

As shown in Fig. 13a the permeance of the Poylactive sample seems to be independent of membrane orientation. Minor deviations are presumably caused by the fact that different samples were used for the 'active2feed' and 'active2perm' configuration. What remains peculiar is the general trend that permeance is independent of activity. Adhesion forces within narrow pores are known to lower saturation pressure. As a consequence condensation might be provoked at pressures significantly below initial saturation pressure. This phenomenon is called capillary condensation. The probability of capillary condensation can be calculated by means of the Kelvin equation [51]. At T=45 °C, activities of a=0.4–0.8 and ideal wetting behavior (contact angle θ = 0 °C) capillary condensation occurs at pore diameters below 2.1–8.5 nm. Considering a static contact angle of θ = 78 °C between water and PAN as it is given in the literature [52] shifts this maximum pore size to 0.4–1.8 nm. This is close to the average pore sizes of 2 nm for PAN supports reported in the literature [53]. If condensation occurs, the membrane interphase will be in direct contact with liquid water. As a consequence any dependence on ambient vapor activity vanishes.

The Mx4-A sample revealed a somehow different behavior. Results of the selective layer facing the feed side are plotted in Fig. 13b. Data points show little influence of permeate activity combined with a large superimposed impact of feed activity. By assuming the same slopes for a change in a_P/a_F regardless of feed activity, permeance can mathematically be described by Eq. (24) (visualized with solid lines).

$$Q = 10,397.2 + 408.1\ \exp(4.7a_F) + 4389.9\frac{a_P}{a_F}. \quad (24)$$

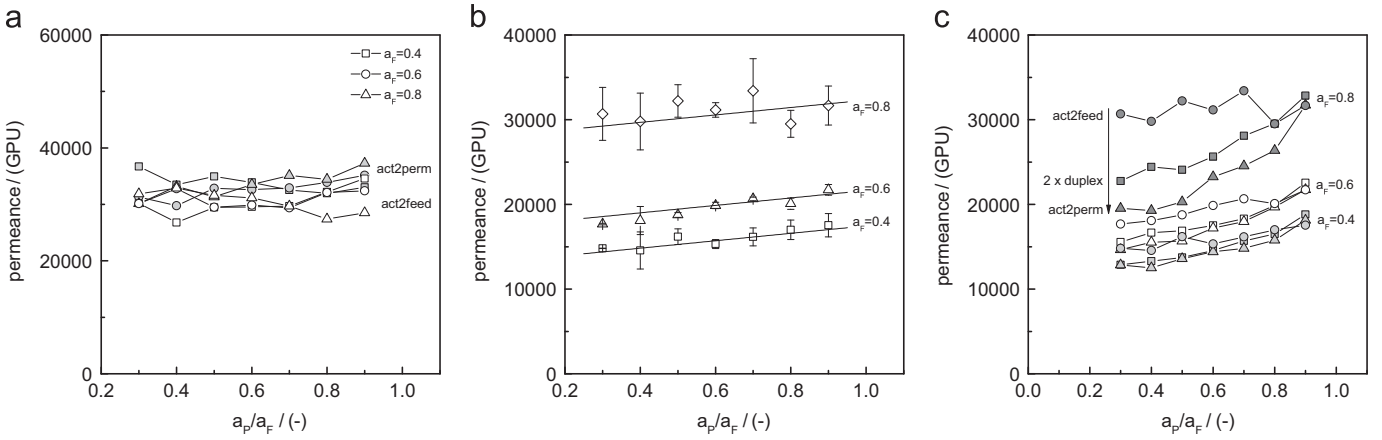

Fig. 13. Water vapor permeances of Polyactive and Mx4-A samples as a function of feed and permeate activity at T=45 °C. (a) Orientation phenomena of the Polyactive sample, (b) activity dependence of the Mx4-A sample with act2feed orientation, (c) orientation phenomena of the Mx4-A sample.

If the orientation of the Mx4-A sample is changed from 'act2feed' to 'act2perm' permeance is affected significantly (Fig. 13c). At $a_F = 0.8$ and a ratio $a_P/a_F = 0.3$ its value decreases approximately 30%. This trend is affirmed by additional experiments with a 'duplex' configuration in which two membranes are sandwiched according to Fig. 12c. Obviously the thickness of this duplex configuration equals twice the thickness of the two other configurations. Thus a mathematical correction is required to directly compare all configurations. Conversion of permeances into permeabilities is not appropriate since the membrane is a composite structure. Normalizing the data with an intrinsic factor (e.g. mean value, highest value) causes a loss of information. For that reason permeances of the duplex configuration were simply doubled. The corresponding values are marked as '2 x duplex' in Fig. 13c. It is important to note that polymer characteristics often change with film thickness and that permeances do not necessarily scale linearly. However the theoretical values of the duplex configuration fit perfectly in between the results of the two other configurations. The results of all three orientations diverge at low permeate activities and merge at permeate activities close to feed activity. While the difference at low permeate activities is peculiar the merging at higher activities could have been expected. If the difference in feed and permeate activity becomes smaller any orientation effects are supposed to disappear. Within the patent describing the membrane assembly it is stated that the selective layer of the membrane is placed on top of a PE-support which contains desiccant particles (preferably silica) [32]. dPoint also reported a change of vapor transmission with membrane orientation. Following their results it depends on temperature and vapor activity which membrane orientation is desirable. Even though it is by far not clarified how to describe the impact of such a desiccant in detail, it is important to know that functionalized substrates are able to cause a change in membrane performance.

An effect which was not considered in the course of this study is pressure loss within the porous substrate. Its impact can be estimated by means of Hagen–Poiseuille, the membrane properties and the process conditions. At high permeabilities a correction of the experimental results might be required in case of dense supports.

6. Conclusions

With the experimental setup and the data sampling shown it is possible to obtain reliable results on membrane permeance as a function of both feed and permeate activity. As discussed in detail three types of activity dependence were observed. While most of the materials (e.g. PFSA, PEBAX) show an increase of permeance with vapor activity, the behavior of PDMS was different. The permeance of PDMS diminished with an increase of permeate activity. At the same time permeance was independent of feed activity.

Within the group of composite materials two different behaviors were obtained. Polyactive and POMS revealed constant permeances over the entire activity range. It is assumed that this behavior can be explained by a predominant influence of the porous support. Some basic calculations revealed the feasibility of capillary condensation and pressure losses within the substrate. Both phenomena were identified as appropriate starting points for further investigations. The impact of functionalized substrates on water vapor permeance was visualized by means of orientation experiments with the Mx4-A sample. The experiments revealed that transport properties can be tuned to a certain extend by implementation of desiccant particles. For future work we propose a systematic variation of desiccant type and load to gain a deeper understanding of functionalized supports.

Acknowledgments

This work was funded by the Federal Ministry for Economic Affairs and Energy on the basis of a decision by the German Bundestag (support code: 03ET1124A). M. Wessling appreciates financial support from the Alexander-von-Humboldt Foundation. In addition to the financial support the authors like to acknowledge the kind donations of membrane samples by FuMa-Tech GmbH, Epurex Films, Paul Waermerueckgewinnung GmbH, dPoint Technologies and Helmholtz-Zentrum Geesthacht. Barbara Dittrich is acknowledged for the supply of the Dehesive PDMS samples.

References

[1] R.W. Baker, K. Lokhandwala, Natural gas processing with membranes: an overview, Ind. Eng. Chem. Res. 47 (2008) 2109–2121.
[2] H. Sijbesma, K. Nymeijer, R. van Marwijk, R. Heijboer, J. Potreck, M. Wessling, Flue gas dehydration using polymer membranes, J. Membr. Sci. 313 (2008) 263–276.
[3] K.L. Wang, S.H. Mccrayb, D.D. Newboldb, E.L. Cussler, Hollow fiber air drying, J. Membr. Sci. 72 (1992) 231–244.
[4] A. Gugliuzza, E. Drioli, A review on membrane engineering for innovation in wearable fabrics and protective textiles, J. Membr. Sci. 446 (2013) 350–375.
[5] K. Kistler, E. Cussler, Membrane modules for building ventilation, Chem. Eng. Res. Des. 80 (2002) 53–64.
[6] L.-Z. Zhang, Heat and mass transfer in a quasi-counter flow membrane-based total heat exchanger, Int. J. Heat Mass Transf. 53 (2010) 5478–5486.
[7] J. Woods, Membrane processes for heating, ventilation, and air conditioning, Renew. Sustain. Energy Rev. 33 (2014) 290–304.
[8] R.S. Prabhakar, R. Raharjo, L.G. Toy, H. Lin, B.D. Freeman, Self-consistent model of concentration and temperature dependence of permeability in rubbery polymers, Ind. Eng. Chem. Res. 44 (2005) 1547–1556.
[9] J. Crank, G.S. Park (Eds.), Diffusion in Polymers, Academic Press, London, 1968.
[10] S.A. Stern, V.M. Shah, B.J. Hardy, Structure–permeability relationships in silicone polymers, J. Polym. Sci.: Part B: Polym. Phys. 25 (1987) 1263–1298.
[11] T.C. Merkel, V.I. Bondar, K. Nagai, B.D. Freeman, I. Pinnau, Gas sorption, diffusion, and permeation in poly(dimethylsiloxane), J. Polym. Sci. : Part B: Polym. Phys. 38 (2000) 415–434.
[12] E. Favre, Experimental evidence and implications of an imperfect upstream pressure step for the time-lag technique, J. Membr. Sci. 207 (2002) 59–72.
[13] H. Lin, B. Freeman, Gas solubility, diffusivity and permeability in poly(ethylene oxide), J. Membr. Sci. 239 (2004) 105–117.
[14] R.W. Baker, J. Wijmans, Y. Huang, Permeability, permeance and selectivity: A preferred way of reporting pervaporation performance data, J. Membr. Sci. 348 (2010) 346–352.
[15] P.M. Hauser, a.D. McLaren, Permeation through and sorption of water vapor by high polymers, Ind. Eng. Chem. 40 (1948) 112–117.
[16] M.J. Thundyil, Y.H. Jois, W.J. Koros, Effect of permeate pressure on the mixed gas permeation of carbon dioxide and methane in a glassy polyimide, J. Membr. Sci. 152 (1999) 29–40.
[17] H. Azher, C.a. Scholes, G.W. Stevens, S.E. Kentish, Water permeation and sorption properties of Nafion 115 at elevated temperatures, J. Membr. Sci. 459 (2014) 104–113.
[18] H. Czichos, T. Saito, L.E. Smith (Eds.), Springer Handbook of Metrology and Testing, 2nd ed.,Springer-Verlag, Berlin, Heidelberg, 2011.
[19] K.A. Schult, D.R. Paul, Techniques for measurement of water vapor sorption and permeation in polymer films, J. Appl. Polym. Sci. 61 (1996) 1865–1876.
[20] D.W. Brubaker, K. Kammermeyer, Apparatus for measuring gas permeability of sheet materials, Anal. Chem. 25 (1953) 424–426.
[21] S. Metz, W. Vandeven, J. Potreck, M. Mulder, M. Wessling, Transport of water vapor and inert gas mixtures through highly selective and highly permeable polymer membranes, J. Membr. Sci. 251 (2005) 29–41.
[22] Standard Test Methods for Water Vapor Transmission of Materials, 2012.
[23] Deutsches Institut für Normung e.V., DIN 53122-1 Prüfung von Kunststoff-Folien - Bestimmung der Wasserdampfdurchlässigkeit, 2001.
[24] C.L. Weller, H. Gooding, Measurement errors in water vapor permeability of highly permeable, hydrophilic edible films, J. Food Eng. 21 (1994) 395–409.
[25] O. Dufaud, E. Favre, L.M. Vincent, Laboratory for gaseous diffusion through permeable solids: the time lag, Chem. Eng. Educ. 34 (2) (2000) 172–177 . 〈http://www.scopus.com/inward/record.url?eid=2-s2.0-0033750929&partnerID=40&md5=fe189c1948d9dc870f3c362f7e5b4051〉. Cited 3 times.
[26] S.W. Rutherford, D.D. Do, Review of time lag permeation technique as a method for characterisation of porous media and membranes, Adsorption 3 (1997) 283–312.
[27] R. Siegel, R. Coughlin, Errors in diffusivity as deducted from permeation experiments using the time-lag technique, J. Appl. Polym. Sci. 14 (1970) 3145–3149.

[28] D. Green, R. Perry (Eds.), Perry's Chemical Engineers' Handbook, 8th ed, McGraw-Hill, New York, 2008.
[29] J.G. Wijmans, R.W. Baker, The solution-diffusion model: a review, J. Membr. Sci. 107 (1995) 1–21.
[30] Y.A. Çengel, M.A. Boles, Thermodynamics: An Engineering Approach, 5th ed., McGraw-Hill, New York, 2005.
[31] J. Potreck, K. Nijmeijer, T. Kosinski, M. Wessling, Mixed water vapor/gas transport through the rubbery polymer PEBAX 1074, J. Membr. Sci. 338 (2009) 11–16.
[32] R.N. Huizing, Coated Membranes for Enthalpy Exchange and Other Applications, US2012/0061045A1, 2012.
[33] S.J. Metz, M.H.V. Mulder, M. Wessling, Gas-permeation properties of poly (ethylene oxide) poly(butylene terephthalate) block copolymers, Macromolecules 37 (2004) 4590–4597.
[34] W. Yave, A. Car, J. Wind, K.-V. Peinemann, Nanometric thin film membranes manufactured on square meter scale: ultra-thin films for CO_2 capture, Nanotechnology 21 (2010) 395301.
[35] T. Brinkmann, J. Pohlmann, U. Withalm, J. Wind, T. Wolff, Theoretical and experimental investigations of flat sheet membrane module types for high capacity gas separation applications, Chemie-Ingenieur-Technik 85 (2013) 1210–1220.
[36] K. Ohlrogge, K. Ebert, Membranen, WILEY-VCH, Weinheim, Germany, 2006.
[37] H. Strathmann (Ed.), Ion-Exchange Membrane Separation Processes, vol. 9, Elsevier, Amsterdam, 2004.
[38] M. Legras, Y. Hirata, Q. Trong, D. Langevin, M. Mtayer, Sorption and diffusion behaviors of water in Nation 117 membranes with different counter ions, Desalination 147 (2002) 7–12.
[39] G. Mauviel, J. Berthiaud, D. Roizard, E. Favre, Dense membrane permeation: From the limitations of the permeability concept back to the solution-diffusion model, J. Membr. Sci. 266 (2005) 62–67.
[40] M. Scholz, M. Alders, T. Lohaus, M. Wessling, Structural optimization of membrane-based biogas upgrading processes, J. Membr. Sci. 474 (2015) 1–10.
[41] T.A. Zawodzinski, C. Derouin, S. Radzinski, R.J. Sherman, V.T. Smith, T.E. Springer, S. Gottesfeld, Water uptake by and transport through Nafion 117 membranes, J. Electrochem. Soc. 140 (1993).
[42] D. Rivin, C.E. Kendrick, P.W. Gibson, N.S. Schneider, Solubility and transport behavior of water and alcohols in Nafion, Polymer (Guildf). 42 (2001) 623–635.
[43] J.a. Barrie, D. Machin, The sorption and diffusion of water in silicone rubbers: Part I. Unfilled rubbers, J. Macromol. Sci. Part B 3 (1969) 645–672.
[44] E. Favre, P. Schaetzel, Q.T. Nguygen, R. Clément, J. Néel, Sorption, diffusion and vapor permeation of various penetrants through dense poly(dimethylsiloxane) membranes: a transport analysis, J. Membr. Sci. 92 (1994) 169–184.
[45] J.A. Barrie, Diffusion in polymers, Trans. Inst. Mar. Eng./C 97 (1985) 79–85.
[46] Y. Yampolskii, I. Pinnau, B. Freeman (Eds.), Materials Science of Membranes for Gas and Vapor Separation, John Wiley & Sons, Chichester, 2006.
[47] S. Metz, J. Potreck, M. Mulder, M. Wessling, Water vapor and gas transport through a poly(butylene terephthalate) poly(ethylene oxide) block copolymer, Desalination 148 (2002) 303–307.
[48] M. Wessling, M. Lidon Lopez, H. Strathmann, Accelerated plasticization of thin-film composite membranes used in gas separation, Sep. Purif. Technol. 24 (2001) 223–233.
[49] Y. Huang, D.R. Paul, Effect of film thickness on the gas-permeation characteristics of glassy polymer membranes, Ind. Eng. Chem. Res. 46 (2007) 2342–2347.
[50] L.-Z. Zhang, A lattice Boltzmann simulation of mass transport through composite membranes, AIChE J. 60 (2014) 3925–3938.
[51] H.-J. Butt, K. Graf, M. Kappl, Physics and Chemistry of Interfaces, WILEY-VCH, Weinheim, 2003.
[52] A. Asatekin, S. Kang, M. Elimelech, A.M. Mayes, Anti-fouling ultrafiltration membranes containing polyacrylonitrile-graft-poly(ethylene oxide) comb copolymer additives, J. Membr. Sci. 298 (2007) 136–146.
[53] N. Scharnagl, H. Buschatz, Polyacrylonitrile (PAN) membranes for ultra- and microfiltration, Desalination 139 (2001) 191–198.